A TRANSTHALAMIC PATHWAY CRUCIAL FOR PERCEPTION

Authors: C. Mo[1,2], C. McKinnon[1], S. M. Sherman[1]
Affiliations: [1]Department of Neurobiology, University of Chicago, Illinois, USA
[2]The Florey Institute of Neuroscience and Mental Health, University of Melbourne, Victoria, Australia

ABSTRACT

Perception arises from activity between cortical areas, first primary cortex and then higher order cortices. This communication is served in part by transthalamic (cortico-thalamo-cortical) pathways, which ubiquitously parallel direct corticocortical pathways, but their role in sensory processing has largely remained unexplored. Here, we show that the transthalamic pathway linking somatosensory cortices propagates task-relevant information required for correct sensory decisions. Using optogenetics, we specifically inhibited the pathway at its synapse in higher order somatosensory thalamus of mice performing a texture-based discrimination task. We concurrently monitored the cellular effects of inhibition in primary or secondary cortex using two-photon calcium imaging. Inhibition severely impaired performance despite intact direct corticocortical projections, thus challenging the purely corticocentric map of perception. Interestingly, the inhibition did not reduce overall cell responsiveness to texture stimulation in somatosensory cortex, but rather disrupted the texture selectivity of cells, a discriminability that develops over task learning. This discriminability was more disrupted in the secondary than primary somatosensory cortex, emphasizing the feedforward influence of the transthalamic route. Transthalamic pathways thus appear critical in delivering performance-relevant information to higher order cortex and are critical hierarchical pathways in perceptual decision-making.

INTRODUCTION

The brain processes sensory signals in hierarchical order with primary sensory cortex activated before secondary cortex (Felleman and Van Essen, 1991). The information from primary to secondary cortex can arrive either directly or indirectly via higher order thalamic nuclei (**Fig. 1A**). These feedforward cortico-thalamo-cortical, or transthalamic, pathways often if not always are present in parallel to direct pathways and use ‘driver’ type synapses that support the fast, robust propagation of stimulus information (Sherman and Guillery, 1998, 2013; Sherman, 2016; Usrey and Sherman, 2021; Miller-Hansen and Sherman, 2022). Feedforward transthalamic pathways are thus well positioned to influence higher order processing. Yet they are absent in most models of perceptual processing (Felleman and Van Essen, 1991; Roland et al., 2014; Hilgetag and Goulas, 2020; Vezoli et al., 2021) and are also absent in standard textbook views of thalamocortical relationships (e.g., Fig. 4.51B of (Luo, 2020), Fig. 28-2 of (Kandel et al., 2000), and Figs. 25.12 and 27.15 of (Squire et al., 2008).

There is some evidence to suggest that these indirect pathways are surprisingly powerful inputs to higher order cortex (Theyel et al., 2010) and carry distinct, task-relevant information, compared to the direct cortical projections (Takahashi et al., 2020; Blot et al., 2021; Yang et al., 2022; Musall et al., 2023). For example, in mice moving through a visual environment, it is the thalamocortical input rather than the corticocortical input that has a stronger influence on the response patterns of higher order cortex (Blot et al., 2021). During a whisker-based perceptual task, activating the transthalamic-projecting cells in primary somatosensory cortex enhanced whisker-based detection, but activating the corticocortical-projecting cells had no behavioral impact (Takahashi et al., 2020). It thus appears that the transthalamic pathway is a key contributor to cortical processing, but it is not clear what information propagates through this pathway to

higher order cortex. Here we show that the feedforward transthalamic pathway is essential for discrimination of stimulus features in cortex and correct perceptual decisions.

We tested the function of the transthalamic pathway in the whisker system of the mouse by using optogenetic inhibition of layer 5 (L5) terminals in higher order thalamus from primary somatosensory cortex (S1). We observed the effects of this inhibition on the animals' ability to perform a whisker-based discrimination task that relies on cortical communication (Helmchen et al., 2018; Park et al., 2022). At the same time, neuronal responses in S1 and secondary somatosensory cortex (S2) were monitored using 2-photon calcium imaging. Importantly, instead of suppressing the pathway during the entire trial (Chen et al., 2016; Qi et al., 2022), which limits interpretation regarding perceptual processing, we separately inhibited during the period of sensory whisking and a delay epoch separating sensation and motor response. We found that texture discrimination performance was impaired by inhibition during both the sensory and delay periods, and inhibition during the sensory epoch also disrupted cell selectivity for the rewarded texture in S2, with smaller effects on cells in S1. Transthalamic pathways thus appear critical in delivering performance-relevant information to higher order cortex and are powerful but underappreciated hierarchical pathways in perception.

RESULTS

BEHAVIORAL EFFECTS OF SUPPRESSING THE TRANSTHALAMIC PATHWAY

Performance on a Discrimination Task

Targeting the somatosensory transthalamic pathway. Cortical L5 cells that project to higher order thalamus are the sources of transthalamic pathways. We selectively inhibited the projection from S1 L5 as follows. We injected a Cre-dependent adeno-associated virus (AAV) carrying the inhibitory opsin, Jaws, into S1 of transgenic mice expressing Cre in layer 5 cells (Rbp4-Cre). An optic fiber was implanted in the higher order thalamic nucleus, the posterior medial nucleus (POm) to inhibit S1 L5 to POm terminals (**Fig. 1B**). The implant was positioned in the anterior-dorsal part of POm, which receives terminals from S1 L5 and contains cells that project to S2 (**Suppl. Fig. 1**) and also cells that project to S1 (Miller-Hansen and Sherman, 2022) We verified Jaws inhibition at these terminals in separate experiments (**Fig. 1B**, **Suppl. Fig. 2**). The impact of inhibition on cortical cells was monitored, thus allowing functional assessment of inhibiting the transthalamic pathway from S1 L5 to POm to S2 or to S1 (**Fig. 1B**).

To locate S1 and S2, we mapped hemodynamic changes to stimulation of the whiskers using intrinsic signal optical imaging of cortex through a cranial glass window (**Fig. 1C**). By overlaying the images of whisker response maps and expression of Jaws-TdTomato in S1 L5, we could exclude any mice with expression that had spread to S2. The overlay also allowed identification of any S1 barrels that did not localize with the expression of Jaws, the corresponding whiskers of which were trimmed. Whiskers that did not contact the texture were left intact. Thus, any whiskers that could contribute to task performance had their neural representation in S1 modifiable by the Jaws opsin.

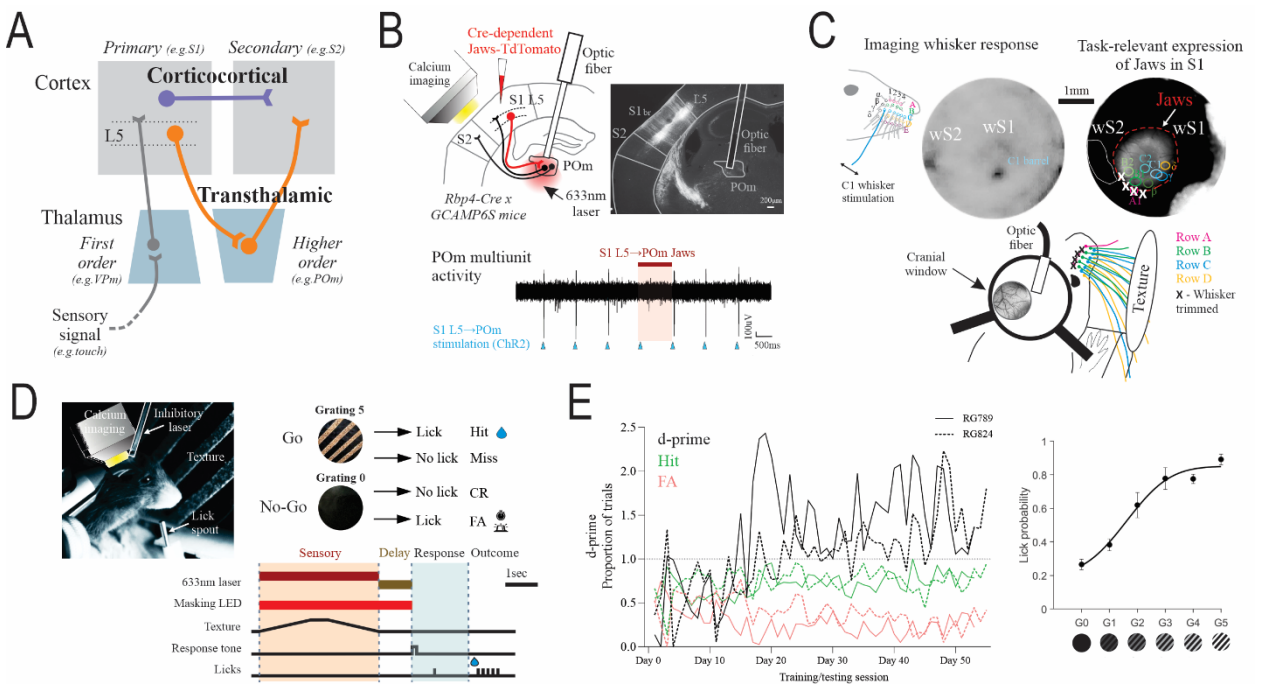

Figure 1. Targeting the somatosensory transthalamic pathway in a discrimination task.
(**A**) Feedforward transthalamic pathways from layer 5 of primary cortex parallel corticocortical projections in perception.
(**B**) (Top left) Expression of the Jaws inhibitory opsin in S1 layer 5 cells and (top right) targeted inhibition via optic fiber implant in anterior POm (see **Suppl. Fig. 1**). The cellular impact was monitored in S1 or S2 by calcium imaging. (Bottom) Example trial of electrophysiological recording in POm showing activation of S1 L5 suppressed by Jaws in POm terminals (see **Suppl. Fig. 2**).
(**C**) (Top left) Functional intrinsic signal optical imaging of whisker-stimulated responses in S1 and S2, viewed through a cranial window. (Top right) For each mouse, areas of S1 that represent individual whiskers ('barrels') were mapped and overlaid with Jaws-TdTomato expression. (Bottom) Any barrels that did not localize with Jaws expression had their corresponding whiskers trimmed (Row A in the example shown; Row E is not shown for clarity). wS1: whisker S1, wS2: whisker S2.
(**D**) (Top) The texture discrimination task followed a go/no-go design where a texture with gratings (G5) was rewarded and a texture of smooth foil (G0) was punished. (Bottom) The task had sensory stimulus, delay and response epochs. For laser inhibition trials, a 633nm laser was activated during either the sensory period or the delay period of the task.
(**E**) (Left) Performance of two example mice during G5 vs G0 discrimination. (Right) Example psychometric performance to various textures during no-laser trials. The G5 texture had gratings made of P20 grit, G4 texture made of P150, G3 of P220, G2 of P1500, G1 of foil strips, and G0 is foil only. Error bars show standard error of the mean.

To test the behavioral effect of inhibiting the S1 L5 to POm projection, we used a texture discrimination task that requires S1 to S2 corticocortical communication (Chen et al., 2016; Helmchen et al., 2018; Park et al., 2022). Textures were presented to the whisker fields of water-restricted, head-fixed mice that indicated their discrimination choice by a lick or no-lick response in a go/no-go task design (**Fig. 1D**). A lick response to a texture with a coarse grating (Grating 5, G5) was rewarded with a drop of water (hit). A lick response to a smooth texture made of foil (Grating 0, G0) was punished with an alarm and 12 sec timeout (False alarm). No-lick responses to G5 were regarded as a miss, whilst no-lick to G0 was a Correct Rejection (CR). A delay of 1 sec separated the texture presentation 'sensory period' of the task from the 'response period' and subsequent 633nm laser to activate Jaws inhibition could be applied during the sensory or delay epochs. Mice generally required 3-4 weeks to successfully discriminate G5 from G0, defined as a d-prime performance above 1 for 2 consecutive days (**Fig. 1E**). Psychometric performance was then probed by presenting various gratings of lower coarseness (G4-G1).

Inhibition of S1 layer 5 to POm terminals impairs discrimination performance. S1 L5 to POm terminals were inhibited with a 633nm laser measured 4 ± 0.2 mW at the tip of the implant in POm (~127mW/mm^2) (**Fig. 2A**). Inhibition during the texture presentation period of the task ("sensory laser") caused higher error rates compared to trials without laser activation ("no-laser") (**Fig. 2B**) Psychometric testing on a range of textures revealed that mice were more likely to lick to the coarser gratings (G3-G5) and less likely to lick to the non-rewarded smooth texture (G0) (**Fig. 2C**, top, black curve). Sensory laser application resulted in a compressed psychometric function (**Fig. 2C**, red curve). Quantification of psychometric curves also reflected an increase in guess rates (false alarm) and lapse rates (miss) (p=0.0078 and p=0.0039, respectively, see **Suppl. Table 1** for additional statistics). The steepness of the psychometric curve (sensitivity) was reduced (p=0.0039) but the discrimination threshold (bias) was not shifted (p=0.92, **Suppl. Table 1**). As another index of performance, we calculated average d-prime for each grating texture compared to the G0 texture. During sensory laser trials, d-prime was reduced for all textures compared to no-laser trials (**Fig. 2C**, bottom). The large effect size of the deficit during sensory laser application was clear when compared to trials performed in the absence of whiskers (**Fig. 2D**).

On separate days, the same mice were also tested on the effects of laser application during the delay period of the task (**Fig. 2E**). This caused a trend to increase error rate (**Fig. 2E**, bottom) and significantly shifted the psychometric curve to the right (**Fig. 2F**, top) with an expected increase in bias (threshold), but no effect on the slope of the curve (p=0.039 and p=0.91 respectively, **Suppl. Table 1**). D-prime performance was reduced during delay laser trials for the textures difficult to discriminate against G0 (G1, G2) but not for those more easily discriminated (G3, G5) (**Fig. 2F**, bottom). Thus, the effect of the laser on performance was significant when applied during the delay epoch but more subtle compared to laser during the sensory period (**Fig. 2D**).

Red light activation in the brain by itself can potentially have effects on mouse behavior through activation of retinal circuits (Danskin et al., 2015; Odoemene et al., 2018). Thus, in addition to a masking LED (Fig. 1D), we performed two controls: One control was to inject mice with AAV carrying TdTomato without Jaws (n=4). These control mice did not show differences between no-laser and sensory laser trials for d-prime, error rate or psychometric curve parameters (**Suppl. Fig. 3A, B**). The same TdTomato-expressing mice were also unaffected by laser application during the delay epoch of the task (**Suppl. Fig. 3C, D**). The TdTomato control group

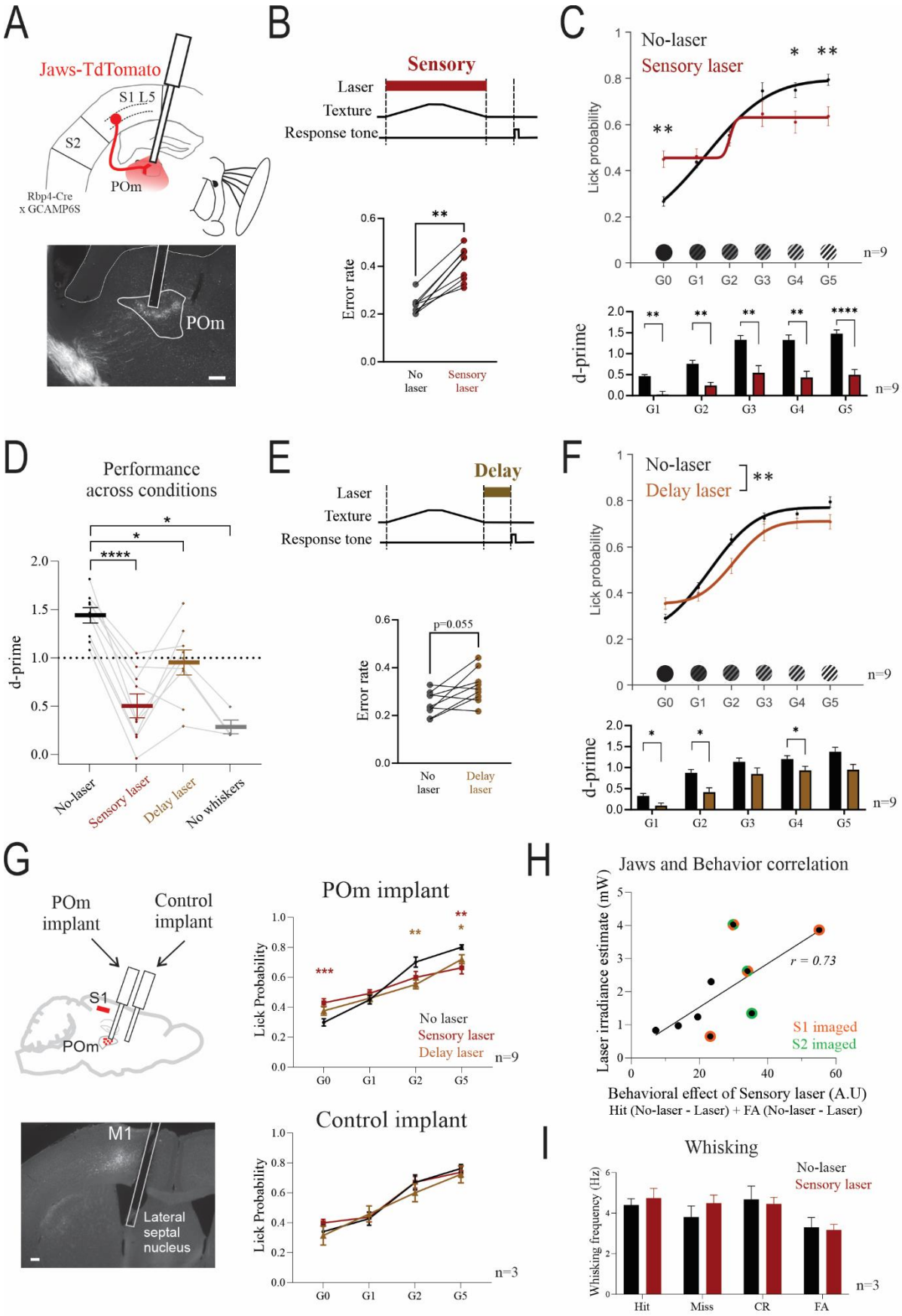
A
Jaws-TdTomato
S1 L5
S2
POm
Rbp4-Cre
x GCAMP6S
POm
B
Sensory
Laser
Texture
Response tone
Error rate
No laser
Sensory laser
C
No-laser
Sensory laser
Lick probability
n=9
G0 G1 G2 G3 G4 G5
d-prime
D
Performance
across conditions
d-prime
No-laser
Sensory laser
Delay laser
No whiskers
E
Delay
Laser
Texture
Response tone
Error rate
p=0.055
No laser
Delay laser
F
No-laser
Delay laser
Lick probability
n=9
d-prime
G
POm
implant
Control
implant
S1
POm
M1
Lateral
septal
nucleus
POm implant
Lick Probability
No laser
Sensory laser
Delay laser
n=9
Control implant
n=3
H
Jaws and Behavior correlation
Laser irradiance estimate (mW)
r = 0.73
S1 imaged
S2 imaged
Behavioral effect of Sensory laser (A.U)
Hit (No-laser - Laser) + FA (No-laser - Laser)
I
Whisking
No-laser
Sensory laser
Whisking frequency (Hz)
Hit
Miss
CR
FA
n=3

Figure 2. Inactivating the S1 L5 projection to POm impairs texture discrimination.

(**A**) (Top) Schematic of S1 L5 to POm terminal inhibition using Jaws opsin during texture discrimination task. (Bottom) Jaws-tdTomato expression and optic fiber implant in an example mouse.

(**B**) (Top) Schematic of sensory laser application during the texture presentation epoch of the task. (Bottom) Error rate for no-laser and sensory laser calculated from the average rate of Miss and FA trials, for G5 and G0 discrimination (9 mice, p=0.0039, paired samples Wilcoxon test).

(**C**) (Top) Psychometric curves for no-laser and sensory laser conditions (n=9 mice from 4-9 sessions each, no-laser vs laser G0: p=0.0078, G4: p=0.017, G5: p=0.0016). (Bottom) D-prime performance across textures for no-laser and sensory laser (n=9 mice, no-laser vs laser G1: p=0.0012, G2: p=0.0065, G3: p=0.0012, G4: p=0.0015, G5: p<0.0001).

(**D**) Averaged d-prime performance across trial conditions (n=4-9 mice from 3-9 sessions each, no-laser vs sensory: p=0.0091, no-laser vs delay: p=0.08, no-laser vs no-whisker: p=0.021, Bonferroni post-hoc tests after mixed effects model).

(**E**) (Top) Schematic of delay laser application between the sensory and response epochs. (Bottom) Error rate for no-laser and delay laser trials (same n=9 mice as sensory laser experiments, p=0.055, paired samples Wilcoxon test).

(**F**) (Top) Psychometric curves for no-laser and delay laser conditions (same n=9 mice as sensory laser averaged from 4-9 sessions each, overall effect of laser p=0.0098, 2-way RM ANOVA, all Bonferroni post-hoc tests p>0.05). (Bottom) D-prime for no-laser vs delay laser (n=9 mice, G1: p=0.023, G2: p=0.048, G3: p=0.10, G4: p=0.029, G5: p=0.11).

(**G**) (Top left) Schematic of a second optic fiber implant targeting an area without Jaws expression. (Bottom left) Example fluorescence image of a control implant in a Jaws-TdTomato-expressing mouse. (Top right) Sensory and delay laser testing within the same session for Jaws-expressing mice with the laser targeting POm (same n=9 mice, averaged from 5-9 sessions each, no-laser vs sensory laser for G5: p=0.0086, G0: p=0.0007, no-laser vs delay laser for G5: p=0.030, G2: p=0.0047, G0: p=0.15). (Bottom right) Sensory and delay laser testing when the laser was attached to the control implant (n=3 mice from 3 sessions each, no effects or interactions found by two-way RM ANOVA).

(**H**) The relationship between the behavioral effect of sensory laser and estimated Jaws terminal activation (see **Methods**) (r: 0.73, p=0.030, Pearson's correlation). The mice which were calcium imaged in S1 (orange) and S2 (purple) are shown (see **Fig. 4**).

(**I**) Whisking analysis during the sensory epoch for no-laser and sensory laser trials (G5 and G0 trials, n=3 sessions from 1 mouse, effect of laser p=0.63, effect of trial p=0.056, Two-way ANOVA).

Values shown as mean ± standard error of the mean. * p<0.05, ** p<0.01, ***p<0.001. All p-values calculated from Bonferroni tests after 2-way repeated measures (RM) ANOVA unless otherwise stated. Scale bars indicate 200μm.

showed that red laser delivery alone did not contribute to the behavioral effects seen in Jaws-expressing mice.

As a second, within-mouse control, 3 of the 9 Jaws-expressing mice expert in the discrimination task were implanted with a second optic fiber, anterior to POm, well away from Jaws-expressing terminals (**Fig. 2G**). The mice were then tested under both sensory and delay laser conditions within the same session using a subset of textures (G0, G1, G2, G5). When the laser was delivered through the POm implant, the effects of sensory and delay laser were replicated (**Fig. 2G**, top right). When the laser was attached to the anterior control implant, there was no effect of laser application on performance (**Fig. 2G**, bottom right). In further support that our laser effects were Jaws-mediated, there was a positive correlation between the errors made during sensory laser (guess and lapse rates) and estimated level of Jaws activation in POm (**Fig. 2H**).

A potential explanation for the impaired ability to discriminate textures during sensory laser could be reduced sensory sampling, that is, reduced whisking of the textures. However, whisker analysis during the sensory period did not show differences in number of whisks between no-laser and sensory laser trials (**Fig. 2I**). A motor-mediated explanation of impaired performance is thus unlikely.

Performance on a Detection Task

In contrast to discrimination, the ability to detect a whisker-based stimulus has been shown to be independent of S1 (Hong et al., 2018; Park et al., 2022) and, as an extension, independent of the S1 L5 transthalamic projection. We tested this hypothesis with the same Jaws-mediated inhibition on a detection task analogous in design to our discrimination task (**Fig. 3A**). Instead of a whisker deflection task with overlapping stimulus and response windows (Takahashi et al., 2016; Yang et al., 2016; Le Merre et al., 2018; Takahashi et al., 2020), we trained mice to detect the deflection of a panel sitting in their whisker field, which was then followed by a 1 second delay before a response cue (**Fig. 3B**). Catch trials of no-movement were presented to test for conditioned licking to the response cue. We trained 4 Jaws-injected mice in the detection task, 3 of which also learnt the discrimination task. Inhibition of the S1 L5 to POm projection shifted the psychometric curve to the right (**Fig. 3C**), increasing the threshold of detection but not affecting sensitivity, lapse and guess rates (**Fig. 3D**). Controls consisted of TdTomato-injected mice (n=3, 1 from discrimination task) and Jaws-injected mice with the laser attached to a second optic fiber implant, as described in the discrimination task (n=2) (**Fig. 2H**). Detection performance in these control mice were no different on laser trials (**Fig. 3E, F**). The impaired detection performance corroborates a study that used inhibitory DREADDs to suppress the projection (Takahashi et al., 2020). However, in contrast to Takahashi et al., we did not find a reduction in response to no-movement catch trials (**Fig. 3C**), which could indicate inhibited responding from the use of DREADDs in general. This is perhaps because optogenetics can be selectively applied to the sensory and delay epochs, avoiding inhibition during the entire trial, including the response period.

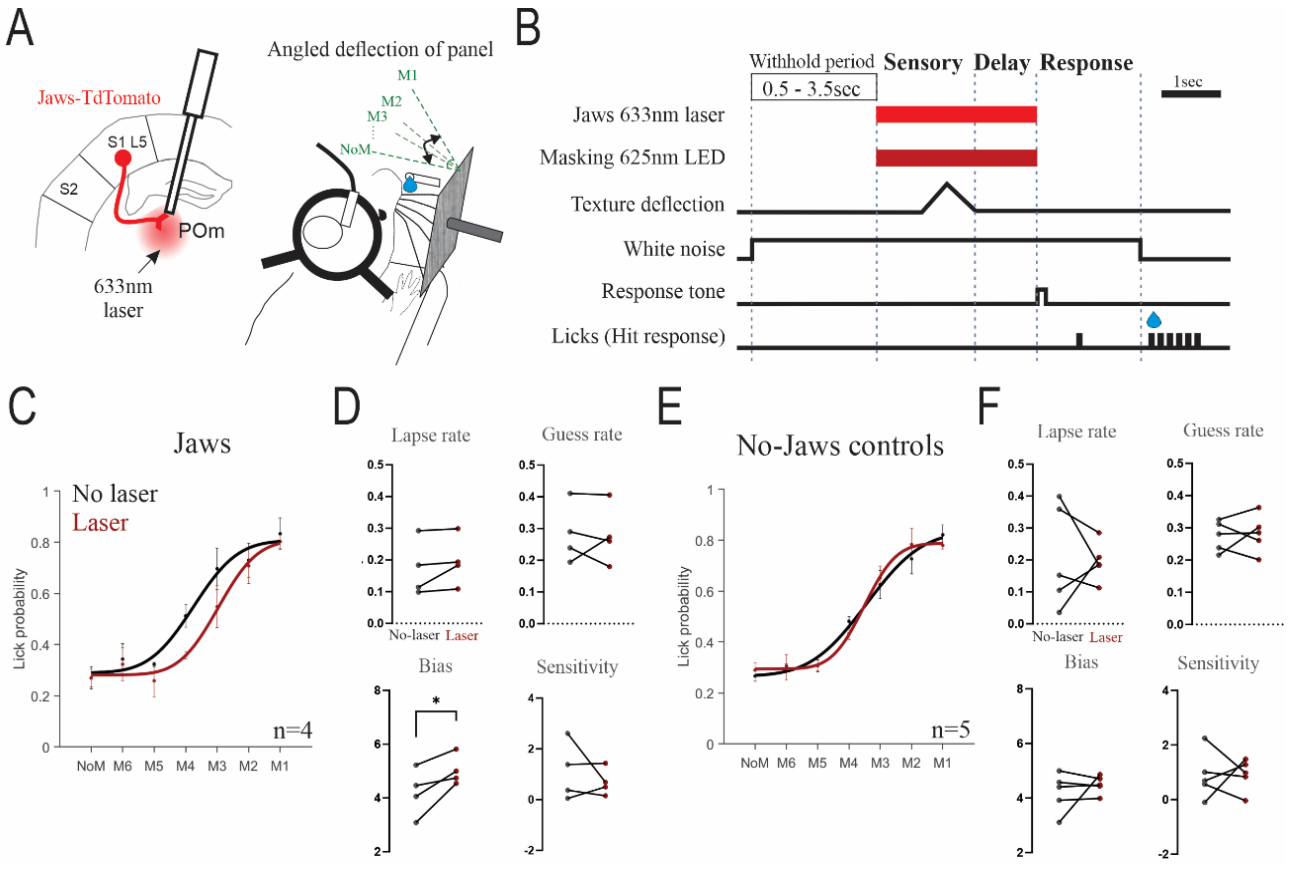

Figure 3. Inhibiting the S1 L5 projection to POm impairs whisker-based detection

(**A**) S1 L5 to POm terminals were targeted for inhibition using the Jaws opsin in Rbp4-Cre mice. Mice were trained to lick at angled movements of a panel located within their whisker field (Hit) and withhold licking to no-movement (NoM) (correct rejection).

(**B**) Time course of a hit trial. A variable pre-movement period reduced prediction of the movement, white noise masked auditory cues and a 625nm LED on every trial habituated the retina to red light. Movement angles M1 – M6 corresponded to 20.5, 13.7, 6.9, 3.4, 1.7, 0.89°.

(**C**) Psychometric fits for performance in mice with Jaws expression (n=4 mice, 3 also learnt the discrimination task). Datapoints for each mouse are an average of 4-6 sessions.

(**D**) Psychometric parameters for the curves in **C**. No-laser vs laser comparisons for lapse rate: p=0.22, guess rate: p=0.91, bias: p=0.048 and sensitivity: p=0.49 (paired t-tests).

(**E**) Same as **C** but for no-Jaws control mice (n=5: 3 TdTomato-expressing mice, 1 of which also learnt the discrimination task, and 2 Jaws mice with control optic fiber implants, which also learnt discrimination). Datapoints for each mouse are an average of 3-6 sessions.

(**F**) Psychometric parameters for curves in **E**. No-laser vs laser comparisons for lapse rate: p=0.83, guess rate: p=0.77, bias: p=0.47 and sensitivity: p=0.96 (paired t-tests).

Error bars show standard error of the mean. * p<0.05.

EFFECTS OF SUPPRESSING THE TRANSTHALAMIC PATHWAY ON CORTICAL RESPONSES

We focused our cortical cell analyses on the discrimination task, the behavior during which we saw the largest effect of transthalamic inhibition (**Fig. 2B,C**). The long decay time of GCAMP6S makes it difficult to isolate cells specifically activated by the delay period, so further analysis is restricted to comparing no-laser and sensory laser trials.

The behavioral impairment resulting from inhibition of S1 L5 to POm terminals could affect encoding in any areas targeted by POm involved in texture discrimination, notably S1 and S2 (Chen et al., 2015; Gilad et al., 2018; Chéreau et al., 2020; Gilad and Helmchen, 2020; Gallero-Salas et al., 2021; Miller-Hansen and Sherman, 2022). To investigate this, we imaged single cell calcium activity using GCAMP6S in layers 2/3 of S1 and S2 in 5 of the 9 Jaws-expressing mice used in the behavioral experiments (**Fig. 4A**).

We limited our analysis to texture responsive cells (see **Methods**) and quantified responsiveness by measuring area under the curve (AUC) of the calcium transient ($\Delta F/F$). A response was defined as the AUC during the sensory period minus that of the pre-stimulus baseline period (**Fig. 4B**). In contrast to silencing all layers of cortex, which reduces cortical responsiveness to a sensory stimulus (Nurminen et al., 2018; Javadzadeh and Hofer, 2022), inhibiting the transthalamic pathway did not affect overall cortical activity in response to texture presentation per se (effect of laser $p=0.11$). In accordance with previous studies on texture discrimination (Chen et al., 2015; Gilad et al., 2018; Chéreau et al., 2020; Gilad and Helmchen, 2020), cells in both S1 and S2 during the no-laser condition showed higher texture responses on G5 hit trials compared to G0 CR trials (**Fig. 4B, C**). Laser inhibition during the sensory period did not affect this preference for the G5 rewarded texture in S1 but disrupted the discrimination in S2 (**Fig. 4C,D**). Hit compared to FA trials was also affected by the laser in S2 but not S1 (**Fig. 4D**)

These data suggest that the transthalamic pathway disrupts the differential response to texture stimuli in S2, and this aligns with disrupted behavioral performance. To further quantify stimulus selectivity, we used receiver-operating characteristic (ROC) curve analysis to calculate a Discrimination Index (DI) for each cell, which expresses the likelihood that an ideal observer correctly classifies trial type (i.e. hit texture vs CR texture), based on the $\Delta F/F$ during the sensory period (**Fig. 4E**) (Chéreau et al., 2020; Gilad and Helmchen, 2020). A permutation test was used to determine if the DI was statistically significant. A positive DI represents selectivity (larger response) for the G5 hit texture and a negative DI represents selectivity for the G0 CR texture. In mice proficient in the discrimination task, the proportion of cells with significant DI (positive or negative) were no different during no-laser and laser conditions, in S1 (no-laser 0.082 vs laser 0.063, $p=0.62$, Wilcoxon test) or S2 (no-laser 0.084 vs laser 0.080, $p=0.87$, Wilcoxon test). However, there was a higher fraction of cells selective for the hit texture compared to the CR texture, in both S1 and S2 (**Fig. 4F**), and laser inhibition disrupted this selectivity in S2. The data also suggest that this is the case in S1 but did not reach a convincing level of statistical significance ($p=0.051$, no-laser vs laser G5 selective fraction) (**Fig. 4F**). We have thus shown that sensory laser application impaired the responsiveness to textures necessary for discrimination selectivity during behavioral performance, particularly in S2 cells (**Fig. 4G**).

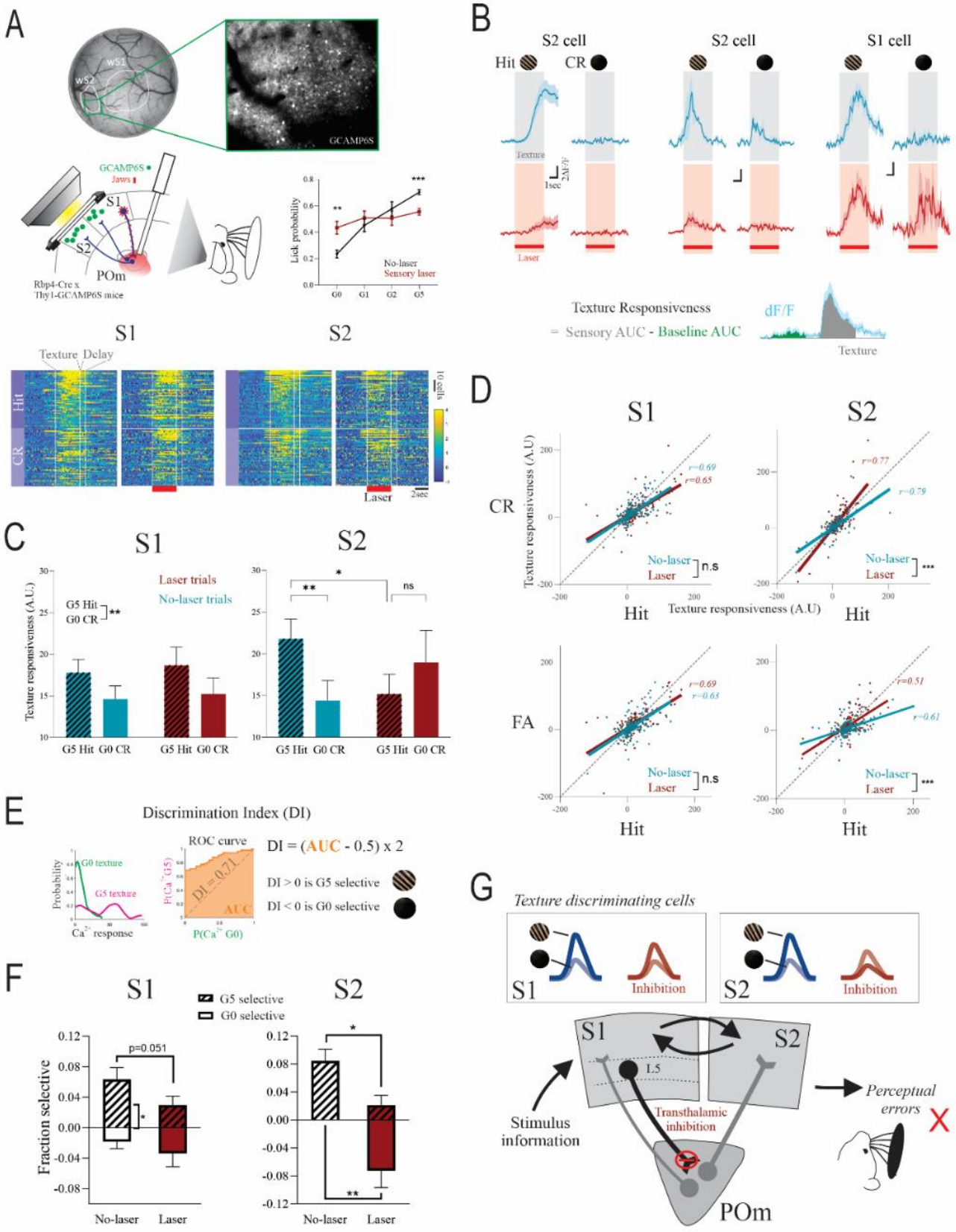
A
wS1
wS2
GCAMP6S
GCAMP6S
Jaws
S1
S2
POm
Rbp4-Cre x
Thy1-GCAMP6S mice
Lick probability
No-laser
Sensory laser
G0
G1
G2
G5
S1
S2
Texture
Delay
Hit
CR
10 cells
Laser
2sec
B
S2 cell
S2 cell
S1 cell
Hit
CR
Texture
1sec
2dF/F
Laser
Texture Responsiveness
= Sensory AUC - Baseline AUC
dF/F
Texture
C
S1
S2
Laser trials
No-laser trials
G5 Hit
G0 CR
Texture responsiveness (A.U.)
G5 Hit G0 CR
G5 Hit G0 CR
G5 Hit G0 CR
G5 Hit G0 CR
D
S1
S2
CR
FA
Texture responsiveness (A.U)
No-laser
Laser
n.s
Hit
Texture responsiveness (A.U)
E
Discrimination Index (DI)
G0 texture
G5 texture
Probability
Ca response
ROC curve
DI = 0.71
AUC
P(Ca G5)
P(Ca G0)
DI = (AUC - 0.5) x 2
DI > 0 is G5 selective
DI < 0 is G0 selective
F
S1
S2
G5 selective
G0 selective
p=0.051
Fraction selective
No-laser
Laser
G
Texture discriminating cells
S1
Inhibition
S2
Inhibition
S1
S2
L5
Stimulus
information
Transthalamic
inhibition
POm
Perceptual
errors

Figure 4. Inhibiting the transthalamic pathway disrupts discriminability of S2 cells with smaller effects on S1 cells.

(**A**) (Top) Schematic of concurrent calcium imaging in S1 or S2 and optogenetic inhibition during texture discrimination. Behavioral performance of imaging trials showed sensory laser effects in hit and CR trials (p=0.0002 and 0.0071 respectively). (Bottom) Example heatmaps of texture-responsive cells during Hit and CR trials, in S1 and S2.

(**B**) (Top) Calcium transients of example cells showing hit and CR discrimination under no-laser (blue) and laser (red) conditions. Grey shading represents texture presentation period. (Bottom) Texture responsiveness value calculation (AUC for texture period - AUC for baseline period).

(**C**) Texture responsiveness for hit and CR trials for no-laser and laser conditions in S1 (left) and S2 (right). For cells inhibited (negative AUC) during no-laser hit trials, AUC values were reversed across trial types. S1: effect of texture p=0.0033, n=240 cells from 7 experiments in 4 mice. S2: no-laser hit vs CR p=0.0013, no-laser hit vs laser hit p=0.032, laser hit vs CR p=0.86 (n=158 cells from 6 experiments in 3 mice, Bonferroni post-hoc test after 2-way RM ANOVA).

(**D**) (Top) Scatterplot of texture responsiveness values for hit vs CR trials in S1 (left) and S2 (right) (S1 no-laser vs laser: p=0.24, n=240 cells, S2 no-laser vs laser: p<0.0001, n=158 cells, linear regression). (Bottom) Scatterplot for hit vs FA trials in S1 (left) and S2 (right) (S1 no-laser vs laser: p=0.59, n=240 cells, S2 no-laser vs laser: p=0.0002, n=158 cells, linear regression).

(**E**) Discrimination index (DI) calculation based on ROC analysis, where positive DI represents G5 texture selectivity and negative DI represents G0 selectivity. Statistical significance was determined using a permutation test. Fraction of significant DI cells for no-laser and laser trials, in S1 (7 experiments, p=0.62) and S2 (6 experiments, p=0.75, Wilcoxon test).

(**F**) Fraction of cells with significant DIs selective for the G5 and G0 textures for no-laser and laser trials, in S1 and S2. S1: no-laser G5 vs no-laser G0 p=0.0164, laser G5 vs laser G0 p=0.27 (McNemar's test), no-laser G5 vs laser G5 p=0.051 (z-test). S2: no-laser G5 vs no-laser G0 p=0.0009, laser G5 vs laser G0 p=0.18 (McNemar's test), no-laser G5 vs laser G5 p=0.025 and no-laser G0 vs laser G0 p=0.0013 (z-test).

(**G**) Schematic of effects of S1 L5 to POm inhibition on texture discriminating cells in S1 and S2.

Values shown as mean ± standard error of the mean. * p<0.05, ** p<0.01, *** p<0.001.

DISCUSSION

Recent evidence suggests that feedforward cortico-thalamo-cortical pathways are distinct and influential routes of sensory processing, compared to direct corticocortical projections (Blot et al., 2021), but many details of their contribution are unknown. To study this further, we inhibited the somatosensory transthalamic pathway at the terminals of S1 L5 to POm whilst monitoring neural activity in S1 and S2, and we found that this had deleterious effects on the ability of the mouse to sense objects by whisking. These perceptual errors coincided with impaired stimulus selectivity of neurons in S2 and to a lesser extent in S1, suggesting a new role of cortico-thalamo-cortical pathways in sensory choice. These causative results extend previous work on the neural basis of texture discrimination and cortical information flow for perceptual decisions.

BEHAVIORAL EFFECTS

The design of our behavioral task allowed us to distinguish effects of inhibiting the transthalamic pathway(s) separately during the sensory sampling period and during a delay period (**Fig. 1)**, rather than silencing throughout the entire behavioral trial (Chen et al., 2013; Takahashi et al., 2020; Park et al., 2022; Qi et al., 2022). We report discrimination deficits due to the inhibition during both periods, albeit to a lesser degree during the delay epoch.

During the Sensory Period

Inhibition during texture presentation severely impaired discrimination performance, increasing total errors, lapse rates and guess rates (**Fig. 2B, C**). This is also likely an *underestimate* of the effects of S1 L5 to POm terminal inhibition, because complete efficiency of Jaws expression in S1 L5 to POm terminals is not feasible, and precisely-targeted probe placements are required for strong behavioral and imaging effects (**Fig. 2H**).

We found deficits due to inhibition of the transthalamic pathway not only on somatosensory discrimination but also on detection (**Fig. 3**). Evidence exists that whisker-based detection can occur in the absence of barrel cortex (Hong et al., 2018; Park et al., 2022) and thus presumably in the absence of the S1 L5 to POm projection. However, others have found that suppressing the S1 L5 projection to POm using chemogenetics impairs tactile detection. Our results suggest that such inhibition impairs performance by increasing the threshold to detect a small movement but does not alter detection of larger ones (**Fig. 3C, D**). Thus, the S1 L5 to POm projection affects detection thresholds rather than detection per se.

During the Delay Period

The behavioral impairment during inhibition of the delay period suggests that transthalamic signaling is ongoing after sensory sampling and contributes to task performance. Interestingly, persistent activity in cortical areas relies on constant input from higher order thalamus for processes such as working memory and premotor planning (Reinhold et al., 2015; Bolkan et al., 2017; Guo et al., 2017). Thus, a simple explanation for this result is that inhibition of the transthalamic pathway, by reducing the input from POm, prevents the establishment of persistent activity in S2. However, it is also plausible that inhibition of this transthalamic processing reduces thalamic input to other cortical regions that may also be involved in this behavior: such potential

cortical targets include association cortices such as M2 (Gilad et al., 2018; Gallero-Salas et al., 2021), which has an S1 L5 transthalamic input (Mo and Sherman, 2019).

By restricting inhibition to the sensory or delay epochs of the task, we avoided any potential confounds of suppressing the ability to report the sensory choice. We also confirmed that optogenetic inhibition did not affect the amount of whisking (i.e. sensory sampling) (**Fig. 2K**), and during the detection task, inhibition did not induce perceived whisker movements during catch trials (**Fig. 3C**). It is thus unlikely that reduced or aberrant motor activity can explain the impaired behavioral performance.

EFFECTS ON NEURONAL RESPONSES

We conclude from the behavioral data that the S1 to POm projection is crucial for somatosensory discrimination, particularly during the stimulus sampling period. S1 and S2 are the cortical origins of perceptual activity during sensory decisions (Kwon et al., 2016; Yang et al., 2016; Esmaeili et al., 2021; Buetfering et al., 2022). This leads to the question: What information is the pathway propagating during this sensory period in these brain regions that is necessary for performance?

Disrupted Texture Discriminability

We investigated this question using 2-photon calcium imaging and concurrent optogenetic inhibition in a subset of the same mice that underwent behavioral testing. In agreement with previous studies, during texture discrimination performance, cells in S1 and S2 show hit/CR discrimination: calcium activity in response to textures during hit trials is higher compared to correct rejection trials (Chen et al., 2013; Chen et al., 2016; Gilad et al., 2018; Gallero-Salas et al., 2021). This selectivity for the hit texture over the unrewarded CR texture is a key correlate of expert discrimination performance and successful reversal learning (Chen et al., 2015; Chéreau et al., 2020; Gilad and Helmchen, 2020). We now show causal evidence that the stimulus texture selectivity is a neural substrate of correct discrimination. Inhibition of the transthalamic projection abolished hit selectivity of the S2 population (**Fig. 4B,C,F**), in alignment with increased performance errors (**Fig. 2B,C, 4A**). However, inhibition did not change the total proportion of texture discriminating cells; instead, it changed the relative proportions of cells selective for either the hit and CR texture (**Fig. 4F**). During inhibition, the S1 cells that showed discriminability during transthalamic inhibition, were equal fractions of those selective for the hit and CR textures (**Fig. 4F**). This equal fraction of hit vs CR selective cells was also found in naïve mice who had not yet learned the task (Chéreau et al., 2020; Gilad and Helmchen, 2020). In S2 however, inhibition induced more cells to be selective for the CR texture compared to hit texture (**Fig. 4F**), causing a reversal of S2 population texture selectivity. This suggests that without a population preference for the salient, behaviorally-relevant reward stimulus, correct behavioral performance is no longer supported (**Fig. 4J**).

Disruption of S2 discriminability. During multiple days of initial task learning or reversal learning, mechanisms of plasticity and reorganization of connectivity have been implicated in supporting changes in discriminability (Banerjee et al., 2020; Chéreau et al., 2020; Poort et al., 2022). However, optogenetic inhibition occurs on a trial-by-trial basis and the effect of inhibition on population discriminability may be better explained by top-down modulation over shorter timescales (Poort et al., 2022). For example, stimulus discriminability may depend on integrating

sensory and reward inputs in S1, which are then encoded by its L5 outputs. As such, reward signals have been demonstrated in the dendrites of S1 L5 cells (Lacefield et al., 2019), the inhibition of which blocks reward-based learning (Schoenfeld et al., 2022). Thus, the transthalamic pathway may deliver trial-by-trial information on the salience of stimuli to POm for subsequent propagation to S1 and higher order cortex. This transmission of cortical information through POm may allow integration with subcortical information and inhibitory control (Trageser and Keller, 2004; Lavallée et al., 2005; Groh et al., 2014).

Differential effects of inhibition on S1 and S2. A potential explanation for the smaller effects in S1 cells is that the optic fiber, and thus the inhibition, targeted the POm cells that project to S2, and not to S1. However, data from single cell tracing suggest that a POm cell that projects to S2, also branches to innervate S1 (Deschênes et al., 1998; Ohno et al., 2012). Another consideration is that we report effects of inhibition on cells in layers 2/3, where calcium imaging was performed, whereas POm axons mainly target layer 5A and layer 1 of S1 and layer 4 of S2. However, the location of presynaptic terminations is not necessarily where the postsynaptic cell body resides, and indeed, neurons in layer 2/3 of S1 receive a major monosynaptic input from POm (Viaene et al., 2011; Oh et al., 2020), despite their terminations avoiding this layer (Sermet et al., 2019). Thus, the transthalamic pathway innervates layer 2/3 cells in S1, but inhibiting the pathway did not have as robust effects on these cells, compared to layer 2/3 cells in S2. This result makes sense in a hierarchical framework, where the POm to S1 pathway is considered feedback and that from POm to S2 is considered feedforward (Miller-Hansen and Sherman, 2022). It also makes sense at a synaptic level, where POm to S1 glutamatergic projections have synaptic properties that modulate the post-synaptic cell (Viaene et al., 2011), whereas POm to S2 synapses are all fast, robust, all-or-none projections, termed 'driver' projections (Miller-Hansen and Sherman, 2022). Driver projections are those that deliver stimulus information (Sherman and Guillery, 1998, 2013; Usrey and Sherman, 2021).

Direct Corticocortical Versus Transthalamic Pathways in Perceptual Tasks

Cortical inhibition experiments have shown that S1 and S2 are critical for somatosensory decisions (Hong et al., 2018; Esmaeili et al., 2021; Park et al., 2022). However, it is important to note that these silencing strategies also inhibit transthalamic pathways through cortical L5. The severe performance deficits we report here from corticothalamic inhibition occurred in the presence of functional corticocortical pathways. Transthalamic inhibition neither acted to reduce overall neural activity nor changed the fraction of texture discriminating cells in cortex. The impact of inhibition was specific to the neural activity relevant for correct behavior. Studies that compare the role of corticocortical projections and corticothalamic projections in sensory decisions show that corticothalamic pathways make a larger contribution to performance (Takahashi et al., 2020; Musall et al., 2023). Our results add to the mounting evidence suggesting that perceptual processing in cortex may be largely supported by transthalamic signaling.

CONCLUSIONS

In summary, we have presented behavioral and neuronal data that causally implicate the transthalamic pathway in propagating stimulus feature selectivity for correct perceptual decisions.

Our results demonstrate the need to include transthalamic circuits and higher order thalamus in the framework for cortical functioning in perception.

METHODS

ANIMALS

All experiments were performed in accordance with protocols approved by the Institutional Animal Care and Use Committee at the University of Chicago. Transgenic mice expressing Cre-recombinase in L5 of cortex (Rbp4-Cre) (Gerfen et al., 2013) were bred by crossing hemizygous male Tg(Rbp4-Cre) KL100GSat/Mmcd mice (GENSAT RP24-285K21) with female C57Black6J mice. Rbp4-Cre positive offspring were used for *in vivo* electrophysiology experiments (**Suppl. Fig. 2**). All other data were generated with Rbp4-Cre x Thy1-GCAMP6S mice, created by breeding male Rbp4-Cre mice with female Thy1-GCaMP6S mice (GP4.12Dkim/J, Stock: 025776, The Jackson Laboratory). Tail biopsies were taken at 14-21 days old and genotyped by real time polymerase chain reaction (Transnetyx, Cordova, TN). Mice used in behavioral experiments were a balanced mix of male and female and housed individually on a reverse light-dark cycle (7am-7pm). All mice were given food and water *ad libitum*, unless water restricted as described.

SURGICAL PROCEDURES

Mice were anaesthetized with ketamine (100 mg/kg)/xylazine (3 mg/kg, i.p) and maintained on isoflurane (1.0-1.5% in oxygen). A small burr hole was made over the target site and virus was injected using a 0.5uL syringe (7000.5KH, Hamilton) at a rate of 5-10nl/min. To express Jaws-TdTomato or TdTomato alone in L5 of S1, 250nl of AAV8-CAG-FLEX-Jaws-KGC-TdTomato-ER2 (UNC Vector Core) or AAV5-CAG-FLEX-TdTomato (UNC Vector Core) was injected into left S1 of 6 week old mice. S1 coordinates relative to bregma were DV: −0.5, ML: 3.2mm, AP: -1.3mm. After 2 weeks, a custom titanium head post (11.5mm diameter, H.E. Parmer) was adhered to the skull using dental cement (C&B Metabond). In the same surgery, a 4mm circular cranial window (0.66mm thick, Tower Optical) attached to a 5mm glass coverslip was implanted over S1 and S2 (DV: −0.5, ML: 4.2mm, AP: -1.2mm). An optic fiber stub (200µm diameter, 0.5NA, Thorlabs) was also implanted at 8° from the vertical to target left POm (DV: -3.15mm, ML: 0.85mm, AP: -1.25mm). In three mice, a second optic fiber was implanted subcortically, anterior to POm after behavioural training. After all surgeries, analgesia (Meloxicam, 1-2mg/kg, s.c) was administered pre-operatively and 24 hours post-operatively.

INTRINSIC SIGNAL OPTICAL IMAGING

S1 and S2 were functionally located in each mouse using intrinsic signal optical (IS) imaging. Mice were anesthetized with 3% isoflurane in oxygen and maintained on 1% isoflurane. Reflected light through the cortical window was imaged using a CCD camera (Teledyne QImaging, Retiga-SRV). The surface vasculature was visualized under green illumination (525nm) and hemodynamic response was captured under red illumination (625 nm). Multi-whisker responses were stimulated with a textured panel (3Hz antero-posteriorly, 2cm from the whisker

pad). Single whiskers were threaded with a pipette tip for stimulation (5Hz antero-posteriorly). Images were acquired with custom MATLAB code 1 second after stimulus application (4 second duration), and alternated with no-stimulation trials (30 trials each, 8 seconds inter-trial interval). The signal was quantified as the difference in the reflected light during the stimulus trials and no-stimulus trials.

Trimming to task-relevant whiskers

For each mouse, the whisker map generated from IS imaging was overlaid with the fluorescence image of Jaws-TdTomato. If the S1 barrels of task-relevant whiskers did not express Jaws-TdTomato, the corresponding whiskers were trimmed down to the whisker pad (**Fig. 1C**). Task-relevant whiskers were verified for each mouse as those which consistently came into contact with the texture panel during the discrimination task (typically alpha, A1, beta, B1, B2, gamma, C1, C2, delta, D1, and D2 whiskers). Whisker length was monitored every 3-4 days and re-trimmed as necessary.

Behavioral Setup and Discrimination Task

Set up

The behavioral enclosure was lightproof and fitted with soundproof panels (0.8 NRC, Sound Seal) with the following internal light sources: An infrared webcam (webcamera_usb) and a 625nm LED (Thorlabs) with the output diffused with an acrylic panel and Kimwipe tissues. The 625nm LED was positioned 20cm in front of the mouse's face and emitted during the sensory period of every trial. Speakers were positioned so the response tone (8kHz, MATLAB) was 60dB at the distance of the mouse. A pump (NE-1000 syringe pump, New Era) delivered water through a spout (15G blunt needle) mounted 3-6mm away from the mouth. Licks were detected by an attached capacitance sensor (Teensy 3.2, PJRC). Mice were able to run freely on a custom-built treadmill.

Textured panels (5.5cm diameter circles) were attached to a custom-built 8-sided wheel (7cm radius), rotated by a stepper motor (X-NMS17C, Zaber). Textures were presented one at a time to the mouse by mounting the stepper motor vertically on a linear slider (X-LSM050, Zaber) and advancing it into, and retracting it out of, the right whisker field. At the start of each trial, the wheel was rotated in either direction for a random amount of time (0.34 - 1.8 seconds) to prevent predictive auditory cues. The linear slider advanced the texture from 3.7cm from the whisker pad, to 2.2cm away, still out of reach of most whiskers, and then into the whisker field, 1.2cm away from the pad. The texture was held at this position for 0.5 seconds and retracted, upon which there was a delay period (0.6-1 seconds), followed by the tone and response period. Synchronization and triggers were controlled through MATLAB (2020b).

Habituation

One week after window surgery, mice were water restricted to 80-95% weight and habituated to the head-fix apparatus within the enclosure over 3-5 days. During the habituation period, mice were first encouraged to lick the spout (8uL water delivery). Then, water delivery

was paired with a preceding tone (8kHz) until mice self-triggered the delivery by licking the spout within 2 seconds of the tone onset.

G5 and G0 discrimination training

Mice were then trained on a go/no-go design to discriminate between a smooth texture (no-go: matte, black, aluminum foil) and one with a grating (go: gratings on foil). The grating textures were made of 5mm-wide sandpaper strips, 7mm apart on black foil. During initial training, the presentation of a grating texture (P20 grit strips: G5 texture) was associated with a water reward (6uL). For the first few G5 trials, water delivery was triggered immediately after the response tone. Then, water was only delivered if mice licked the spout after the tone, but within the response period (1.8 seconds). Water delivery only occurred after the end of the response period. Licking during the delay period triggered one alarm beep (NE-1000 syringe pump, New Era), aborting the trial for immediate restart.

If the mouse licked during the response period of a G5 trial, the trial was deemed a "hit". No-lick response to the G5 texture during the response period was regarded a "miss". If the mouse performed 3 hit trials in a row, then the no-go G0 texture was introduced. Licking during the response period to the G0 texture triggered a beeping alarm (65dB, NE-1000 syringe pump) and 12 second timeout ("false alarm", FA). If mice correctly withheld a lick response to the G0 texture, this was a "correct rejection" (CR) and punishment was avoided. If the previous two G0 textures were FAs, a mild air puff to the snout region was also administered (Cleaning duster, Office Depot). The consequence for a miss and CR response was moving to the next trial. G5 and G0 textures were presented in random order but with not more than 2 in a row and the inter-trial interval was 3-5 seconds.

During training, the 0.6 second delay period was extended to 1 second and the response period shortened from 2 to 1.6 seconds. Mice were considered trained when performance reached a d-prime of >1 or >70% correct for two consecutive days. On training and testing days, mice were allowed to perform the task until sated and then supplemented in their home cage with 0-0.8ml water to maintain a body weight of 80-95%.

Psychometric and laser testing

After learning to discriminate G5 and G0, textures of various coarseness were presented in randomized order (G4=P100, G3=P220, G2=P1500, G1=foil strips on foil) in addition to G5 and G0. G0 was presented on 30% of trials. Effects of the laser (see **Optogenetic inhibition**) were initially tested during two conditions, in separate testing sessions on alternate days: 1) laser during the sensory period (3.8 seconds) 2) laser during the delay period (1 second). For each session, laser and no laser trials were presented at 50% each, except when the mouse was returned to G0 and G5 training (see **Bias correction**). In a third testing condition, both sensory laser trials and delay laser trials were tested in the same session but only textures G0, G1, G2 and G5 were presented. This testing was used during 2-photon imaging. Behavioral sessions were run daily and typically consisted of 150–400 trials lasting between 1 - 2 hours. Only sessions during which mice performed for no-laser trials (d-prime>1 or >70% correct) were included in the analyses.

Bias correction

To combat the high bias towards go responses during the beginning of each session (Berditchevskaia et al., 2016), mice are minimally water restricted where possible (80-95%) and given "warm-up" training on G5 vs G0 discrimination. To proceed to psychometric testing, mice must respond to randomized G0 presentations with three CRs in a row (no FAs), which typically required 7-150 trials. Mice are returned to G5 vs G0 training if they perseverate (lick at every trial) or disengage (no lick response) on a sliding window of 7 trials. Any G5 v G0 bias correction trials were excluded from analyses.

Behavioral analyses

Correct performance was calculated for each session from G5 and G0 trials, by the formula:

$$(\text{hit trials} + \text{CR trials}) / (\text{hit} + \text{CR} + \text{miss} + \text{FA trials}) \times 100$$

D-prime was calculated by the difference in z transforms of G5 hit rate and FA rate:

$$d' = z(\text{hit}) - z(\text{FA})$$

Error rate was calculated by taking the average of mean miss trials during G5 presentation and mean FA trials. For each laser testing condition in each mouse, psychometric curves were fitted with a 4-parameter sigmoidal cumulative gaussian function (Wichmann and Hill, 2001):

$$y(x) = g + (1 - g - l) * 0.5 * (1 + \mathrm{erf}((x - u)/\mathrm{sqrt}(2*v^2)))$$

where y(x) is the lick probability, x is the texture and erf represents the error function. The parameters to be fitted are: g (guess rate), l (lapse rate), u (subject bias), and v (discrimination sensitivity).

To plot the relationship between the behavioral effect and Jaws activation for each mouse (**Fig. 2H**), the additive difference between the guess and lapse rates during no-laser and sensory laser trials was plotted against an estimation of laser irradiance, relative to Jaws terminal activation. This laser irradiance was calculated by multiplying the area of Jaws terminal expression in the brain section with the deepest implant location, by the estimated irradiance loss from the tip of the implant to the middle of the expression site (https://web.stanford.edu/group/dlab/cgi-bin/graph/chart.php, 630nm, 0.5NA, 4mW, 0.1mm fiber radius).

Optogenetic Inhibition

Optic fiber implants (200µm diameter, 0.5NA, Thorlabs) were attached to a patch cable (0.5NA, Plexon) to deliver a 633nm laser (LuxX 633-100, Omicron-Laserage) with an estimated power output of 4 ± 0.2 mW. To reduce fluorescence artefacts of the laser during 2-photon imaging, autofluorescence from the patch cable was removed by photobleaching overnight using a 620nm LED (PlexBright, Plexon, 3.5-5mW at tip). During imaging, the red channel photomultiplier tube (PMT) was shuttered closed.

Whisker Tracking

Whisker movements were recorded from above using a CMOS high-speed camera at 122fps (Basler acA800-510um). The whiskers were illuminated with light from an IR camera and white cardboard provided background contrast. However, light levels were not increased for optimal tracking to avoid interfering with concurrent calcium imaging. Thus, whiskers could only be successfully tracked for a subset of sessions. We modified available code (https://github.com/jvoigts/whisker_tracking) based on a convolutional neural network to label whiskers and a hough transform to extract whisker positions and angles (https://github.com/sdemyanov/ConvNet). Analysis was restricted to movements from multiple rows of whiskers within 2cm of the whisker pad during the texture presentation period of the task for G5 (hit and miss) and G0 (CR and FA) trials. A whisk was defined as a continuous sweep > 25 pixels in the antero-posterior axis. The rate of whisking was calculated by the number of whisks / sensory period (3.84 seconds).

Detection Task

In the same behavioral set up as the discrimination task, mice were trained to detect the movement of a textured panel (P20 sandpaper) positioned within the whisker field (1.5cm from the whisker pad). The panel was mounted to the same texture wheel used in the discrimination task. The panel was deflected anteriorly and immediately returned to its original position.

The task followed a go no-go task design, but here the panel movement was the go rewarded cue and no-movement was the no-go punished cue. To minimize timed prediction of a movement, a randomized "withhold" period of 0.5 – 3.5 seconds preceded the deflection. If mice licked during this period, an alarm beep would sound (New Era) and the trial was aborted and restarted. White noise (MATLAB) throughout the trial masked auditory cues from the stepper motor. There was a 1 second delay after the sensory period (panel movement) but before the response tone (8kHz). Licks during the delay period also aborted the trial for restart. Mice are free to move on a treadmill.

Mice were first trained to lick to the largest movement (M1: 20.5°) compared to no-movement (NoM: 0°) and considered trained when performance reached d-prime of >1 or >70% correct for two consecutive days. This typically required 3-7 days. Psychometric and laser testing was then conducted with a range of angles: M2 – M6 corresponding to 13.7, 6.9, 3.4, 1.7, 0.89°. A 625nm LED was emitted during the sensory and delay periods of every trial. The 633nm laser was applied throughout the sensory and delay periods of the task. Behavioral analyses followed that of the discrimination task.

Two-Photon Calcium Imaging

GCAMP6S activity from Rbp4-Cre x Thy1-GCAMP6S mice was excited through a 16X objective (0.8NA, Zeiss) using a Ti:Sapphire laser (DeepSee, Spectra-Physics) tuned to 920 nm. PrairieView software controlled a resonant scanner of a multiphoton microscope (Ultima Investigator microscope, Bruker). Fluorescence was collected through a green emission filter (et525/70m-2p, Chroma Tech, VT, USA) and detected by a GaAsP PMT (Hamamatsu Model H10770). Image sequences over a 512 x 512 µm field of view were captured at 7.5 Hz in layer 2/3.

Each imaging session targeted S1 or S2, which were located through the cranial window based on blood vessel landmarks and whisker mapping results (see **Intrinsic signal optical imaging**). The border area was avoided. In animals imaged more than once, no areas overlapped and only cells imaged in one session were included in the analyses. Five mice in total were imaged in both S1 and S2. However, in 3 mice, analyses were restricted to one region each due to poor GCAMP6S signal, occlusion of the window or not enough behavioral trials.

Image processing

Raw fluorescence images were pre-processed using Suite2p (https://suite2p.readthedocs.io/): regions of interest (ROIs) were selected and their fluorescence signals were extracted and deconvoluted. ROIs fluorescence traces for each experiment were visually confirmed and analyzed using custom MATLAB code. Fluorescence time-series were normalized to percent change from a time-varying baseline ($\Delta F/F$). Baseline fluorescence was estimated for each neuron by thresholding raw fluorescence to eliminate spike-induced fluorescence transients, which was thresholded and smoothed with a 4th-order, 81-point Savitzky-Golay filter (Dechery and MacLean, 2018).

Responsive cells and area under the curve analysis

Each imaging trial included a baseline period of 4 seconds before moving the texture into the whisker field. Responsive cells were defined as ROIs with a significant difference between the mean dF/F during the baseline period compared to the mean dF/F during the texture period, for any G5 and G0 texture trials, including sensory laser trials. Significant difference was determined by a Wilcoxon signed rank test ($p<0.05$) when absolute value skew <0.6 or sign test when absolute value skew >0.6. Only responsive cells were used in subsequent analysis. Due to the slow kinetics of GCAMP6S and long sensory period of the task, we used area under the curve (AUC) of the dF/F trace as a measure of responsivity to the texture presentation. Texture responsiveness value was calculated as the AUC during the sensory period – AUC during the baseline period. Both periods were 3.8 seconds long. To determine the effect of the laser on cells that reduced response to the texture, any cell which showed negative texture responsiveness values during no-laser G5 trials had their other trial responsiveness values reversed in sign (**Fig. 4C**).

Single-neuron discrimination index analysis

To quantify how well single cells could discriminate between the two hit and CR textures, a discrimination index (DI) was calculated based on neurometric functions using a receiver-operating characteristic (ROC) analysis (Chen et al., 2013, Chéreau et al., 2020). AUC of calcium signals during the second half of the stimulus presentation period minus the AUC of an equivalent baseline period in the G5 hit texture trials were compared to that of the G0 CR texture trials. ROC curves were generated by plotting, for all threshold levels, the fraction of G5 hit trials against the fraction of G0 CR trials for which the response exceeded threshold. Threshold levels were defined as a linear function from the minimal to the maximal calcium signals. DI was computed from the area under the ROC curve by: $DI = (AUC - 0.5) \times 2$. DI values vary between -1 and 1. Positive values indicate a larger response, or selectivity, to the G5 hit texture compared to the G0 CR texture, whilst negative values indicate a selectivity to the G0 CR over G5 hit texture. DI values

above chance were assessed using permutation tests, from which a sampling distribution was obtained by shuffling the texture labels of the trials 1,000 times. The measured DI was considered significant when it was outside of the 2.5th–97.5th percentiles interval of the sampling distribution.

Fluorescence Microscopy

Mice were perfused with cold, phosphate buffered saline (pH 7.2, 50ml) followed by cold, 4% paraformaldehyde (100ml). Brains were extracted, sucrose-protected over two days, and sectioned on a sliding microtome. Brain sections were cut 50µm thick and mounted with Superfrost slides. Some fluorescent photos were captured before mouting. Fluorescence signals were visualized under a fluorescence microscope (Leica Microsystems) using the appropriate filter cubes. Images were captured using a Retiga-2000 CCD monochrome camera and QCapturePro imaging software (Teledyne QImaging, Surrey, BC). Image post-processing such as estimating the distance from optic fiber implant (**Fig. 2H**) was performed with ImageJ software.

Statistics

Statistical tests were conducted in MATLAB (2020b) or Prism software (v.9, GraphPad). A Shapiro-Wilk test (<30 samples) or Kolmogorov Smirnoff test (>30 samples) was used to test for normality. If no significant departure from normality was found, parametric tests were used. For departures from normality, the non-parametric Wilcoxon signed rank test was used for unpaired values and the Wilcoxon matched-pairs signed rank test for paired values. Where normality differed for tests within an experiment, the more conservative non-parametric test was applied across the experiment for consistency. A significance level was set at 0.05 and multiple comparisons were adjusted with the Bonferroni correction unless otherwise indicated. Specific statistical tests used and sample sizes are indicated in figure legends, text and **Suppl. Table 1**.

ACKNOWLEDGEMENTS

We thank Masaki Makitani, Adam Kunz, Jessica Manieson and Graham Fetterman for their technical assistance, and Jackson Cone for comments on drafts of the manuscript. This work was supported by the National Institutes of Health (Grants NS094184 and EY022388 to S.M.S. and F31EY031965 to C.McK.) and the National Health and Medical Research Council, Australia (Grant 2003646 to C.M.).

AUTHOR CONTRIBUTIONS

C.M. and S.M.S. conceived the project and wrote the manuscript. C.M. performed the experiments, C.M. and C.McK. performed the analyses.

REFERENCES

Banerjee A, Parente G, Teutsch J, Lewis C, Voigt FF, Helmchen F (2020) Value-guided remapping of sensory cortex by lateral orbitofrontal cortex. Nature 585:245-250.

Berditchevskaia A, Cazé RD, Schultz SR (2016) Performance in a GO/NOGO perceptual task reflects a balance between impulsive and instrumental components of behaviour. Sci Rep 6:27389.

Blot A, Roth MM, Gasler IT, Javadzadeh M, Imhof F, Hofer SB (2021) Visual intracortical and transthalamic pathways carry distinct information to cortical areas. Neuron 109:1996-2008.

Bolkan SS, Stujenske JM, Parnaudeau S, Spellman TJ, Rauffenbart C, Abbas AI, Harris AZ, Gordon JA, Kellendonk C (2017) Thalamic projections sustain prefrontal activity during working memory maintenance. Nature neuroscience 20:987-996.

Buetfering C, Zhang Z, Pitsiani M, Smallridge J, Boven E, McElligott S, Häusser M (2022) Behaviorally relevant decision coding in primary somatosensory cortex neurons. Nat Neurosci 25:1225-1236.

Chen JL, Carta S, Soldado-Magraner J, Schneider BL, Helmchen F (2013) Behaviour-dependent recruitment of long-range projection neurons in somatosensory cortex. Nature 499:336-340.

Chen JL, Voigt FF, Javadzadeh M, Krueppel R, Helmchen F (2016) Long-range population dynamics of anatomically defined neocortical networks. eLife 5.

Chen JL, Margolis DJ, Stankov A, Sumanovski LT, Schneider BL, Helmchen F (2015) Pathway-specific reorganization of projection neurons in somatosensory cortex during learning. Nature neuroscience 18:1101-1108.

Chéreau R, Bawa T, Fodoulian L, Carleton A, Pagès S, Holtmaat A (2020) Dynamic perceptual feature selectivity in primary somatosensory cortex upon reversal learning. Nature communications 11:3245.

Danskin B, Denman D, Valley M, Ollerenshaw D, Williams D, Groblewski P, Reid C, Olsen S, Blanche T, Waters J (2015) Optogenetics in mice performing a isual discrimination task: measurement and suppression of retinal activation and the resulting behavioral artifact. PLoS One 10:e0144760.

Dechery JB, MacLean JN (2018) Functional triplet motifs underlie accurate predictions of single-trial responses in populations of tuned and untuned V1 neurons. PLoS Comput Biol 14:e1006153.

Deschênes M, Veinante P, Zhang ZW (1998) The organization of corticothalamic projections: reciprocity versus parity. Brain Research Reviews 28:286-308.

Esmaeili V, Tamura K, Muscinelli SP, Modirshanechi A, Boscaglia M, Lee AB, Oryshchuk A, Foustoukos G, Liu Y, Crochet S, Gerstner W, Petersen CCH (2021) Rapid suppression and sustained activation of distinct cortical regions for a delayed sensory-triggered motor response. Neuron 109:2183-2201.e2189.

Felleman DJ, Van Essen DC (1991) Distributed hierarchical processing in the primate cerebral cortex. CerebCortex 1:1-47.

Gallero-Salas Y, Han S, Sych Y, Voigt FF, Laurenczy B, Gilad A, Helmchen F (2021) Sensory and behavioral components of neocortical signal flow in discrimination tasks with short-term memory. Neuron 109:135-148.e136.

Gerfen CR, Paletzki R, Heintz N (2013) GENSAT BAC cre-recombinase driver lines to study the functional organization of cerebral cortical and basal ganglia circuits. Neuron 80(6):1368-1383.

Gilad A, Helmchen F (2020) Spatiotemporal refinement of signal flow through association cortex during learning. Nature communications 11:1744.

Gilad A, Gallero-Salas Y, Groos D, Helmchen F (2018) Behavioral strategy determines frontal or posterior location of short-term memory in neocortex. Neuron 99:814-828.e817.

Groh A, Bokor H, Mease RA, Plattner VM, Hangya B, Stroh A, Deschenes M, Acsády L (2014) Convergence of cortical and sensory driver inputs on single thalamocortical cells. Cereb Cortex 24:3167-3179.

1014 Guo ZV, Inagaki HK, Daie K, Druckmann S, Gerfen CR, Svoboda K (2017) Maintenance of persistent
1015 activity in a frontal thalamocortical loop. Nature 545:181-186.
1016 Helmchen F, Gilad A, Chen JL (2018) Neocortical dynamics during whisker-based sensory discrimination
1017 in head-restrained mice. Neuroscience 368:57-69.
1018 Hilgetag CC, Goulas A (2020) 'Hierarchy' in the organization of brain networks. Philosophical transactions
1019 of the Royal Society of London Series B, Biological sciences 375:20190319.
1020 Hong YK, Lacefield CO, Rodgers CC, Bruno RM (2018) Sensation, movement and learning in the absence
1021 of barrel cortex. Nature 561:542-546.
1022 Javadzadeh M, Hofer SB (2022) Dynamic causal communication channels between neocortical areas.
1023 Neuron 110:2470-2483.e2477.
1024 Kandel ER, Schwartz JH, Jessell TM (2000) Principles of Neural Science. New York: McGraw Hill.
1025 Kwon SE, Yang H, Minamisawa G, O'Connor DH (2016) Sensory and decision-related activity propagate in
1026 a cortical feedback loop during touch perception. Nature neuroscience 19:1243-1249.
1027 Lacefield CO, Pnevmatikakis EA, Paninski L, Bruno RM (2019) Reinforcement learning recruits somata
1028 and apical dendrites across layers of primary sensory cortex. Cell Rep 26:2000-2008.e2002.
1029 Lavallée P, Urbain N, Dufresne C, Bokor H, Acsády L, Deschênes M (2005) Feedforward inhibitory control
1030 of sensory information in higher-order thalamic nuclei. Journal of Neuroscience 25:7489-7498.
1031 Le Merre P, Esmaeili V, Charrière E, Galan K, Salin PA, Petersen CCH, Crochet S (2018) Reward-Based
1032 Learning Drives Rapid Sensory Signals in Medial Prefrontal Cortex and Dorsal Hippocampus
1033 Necessary for Goal-Directed Behavior. Neuron 97:83-91.e85.
1034 Luo L (2020) Principles of Neurobiology, Second Edition: CRC Press.
1035 Miller-Hansen AJ, Sherman SM (2022) Conserved patterns of functional organization between cortex
1036 and thalamus in mice. Proc Natl Acad Sci U S A 119:e2201481119.
1037 Mo C, Sherman SM (2019) A sensorimotor pathway via higher-order thalamus. Journal of Neuroscience
1038 39:692-704.
1039 Musall S, Sun XR, Mohan H, An X, Gluf S, Li SJ, Drewes R, Cravo E, Lenzi I, Yin C, Kampa BM, Churchland
1040 AK (2023) Pyramidal cell types drive functionally distinct cortical activity patterns during
1041 decision-making. Nature neuroscience.
1042 Nurminen L, Merlin S, Bijanzadeh M, Federer F, Angelucci A (2018) Top-down feedback controls spatial
1043 summation and response amplitude in primate visual cortex. Nature communications 9:2281.
1044 Odoemene O, Pisupati S, Nguyen H, Churchland AK (2018) Visual evidence accumulation guides
1045 decision-making in unrestrained mice. J Neurosci 38:10143-10155.
1046 Oh JY, Han JH, Lee H, Han YE, Rah JC, Park H (2020) Labeling dual presynaptic inputs using cFork
1047 anterograde tracing system. Experimental neurobiology 29:219-229.
1048 Ohno S, Kuramoto E, Furuta T, Hioki H, Tanaka YR, Fujiyama F, Sonomura T, Uemura M, Sugiyama K,
1049 Kaneko T (2012) A morphological analysis of thalamocortical axon fibers of rat posterior
1050 thalamic nuclei: a single neuron tracing study with viral vectors. Cereb Cortex 22:2840-2857.
1051 Park JM, Hong YK, Rodgers CC, Dahan JB, Harano N, Schmidt ER, Bruno RM (2022) Deep and superficial
1052 layers of the primary somatosensory cortex are critical for whisker-based texture discrimination
1053 in mice. bioRxiv:2020.2008.2012.245381.
1054 Poort J, Wilmes KA, Blot A, Chadwick A, Sahani M, Clopath C, Mrsic-Flogel TD, Hofer SB, Khan AG (2022)
1055 Learning and attention increase visual response selectivity through distinct mechanisms. Neuron
1056 110:686-697.e686.
1057 Qi J, Ye C, Naskar S, Inácio AR, Lee S (2022) Posteromedial thalamic nucleus activity significantly
1058 contributes to perceptual discrimination. PLoS biology 20:e3001896.
1059 Reinhold K, Lien AD, Scanziani M (2015) Distinct recurrent versus afferent dynamics in cortical visual
1060 processing. Nature neuroscience 18:1789-1797.

Roland PE, Hilgetag CC, Deco G (2014) Cortico-cortical communication dynamics. Frontiers in systems neuroscience 8:19.

Schoenfeld G, Kollmorgen S, Lewis C, Bethge P, Reuss AM, Aguzzi A, Mante V, Helmchen F (2022) Dendritic integration of sensory and reward information facilitates learning. bioRxiv:2021.2012.2028.474360.

Sermet BS, Truschow P, Feyerabend M, Mayrhofer JM, Oram TB, Yizhar O, Staiger JF, Petersen CC (2019) Pathway-, layer- and cell-type-specific thalamic input to mouse barrel cortex. Elife 8.

Sherman SM (2016) Thalamus plays a central role in ongoing cortical functioning. Nat Neurosci 19:533-541.

Sherman SM, Guillery RW (1998) On the actions that one nerve cell can have on another: Distinguishing "drivers" from "modulators". Proc Natl Acad Sci USA 95:7121-7126.

Sherman SM, Guillery RW (2013) Functional Connections of Cortical Areas: A New View from the Thalamus. Cambridge, MA: MIT Press.

Squire LR, Berg D, Bloom FE, du Lac S, Ghosh A, Spitzer NC (2008) Fundamental Neuroscience, Third Edition: Academic Press.

Takahashi N, Oertner TG, Hegemann P, Larkum ME (2016) Active cortical dendrites modulate perception. Science 354:1587-1590.

Takahashi N, Ebner C, Sigl-Glöckner J, Moberg S, Nierwetberg S, Larkum ME (2020) Active dendritic currents gate descending cortical outputs in perception. Nature neuroscience:10-0677.

Theyel BB, Llano DA, Sherman SM (2010) The corticothalamocortical circuit drives higher-order cortex in the mouse. Nature neuroscience 13:84-88.

Trageser JC, Keller A (2004) Reducing the uncertainty: gating of peripheral inputs by zona incerta. J Neurosci 24:8911-8915.

Usrey WM, Sherman SM (2021) Exploring Thalamocortical Interactions: Circuitry for Sensation, Action, and Cognition. New York: Oxford University Press.

Vezoli J, Magrou L, Goebel R, Wang XJ, Knoblauch K, Vinck M, Kennedy H (2021) Cortical hierarchy, dual counterstream architecture and the importance of top-down generative networks. Neuroimage 225:117479.

Viaene AN, Petrof I, Sherman SM (2011) Properties of the thalamic projection from the posterior medial nucleus to primary and secondary somatosensory cortices in the mouse. Proc Nat Acad Sci Usa 108:18156-18161.

Wichmann FA, Hill NJ (2001) The psychometric function: I. Fitting, sampling, and goodness of fit. Percept Psychophys 63:1293-1313.

Yang H, Kwon SE, Severson KS, O'Connor DH (2016) Origins of choice-related activity in mouse somatosensory cortex. Nat Neurosci 19:127-134.

Yang W, Tipparaju SL, Chen G, Li N (2022) Thalamus-driven functional populations in frontal cortex support decision-making. Nat Neurosci 25:1339-1352.